Int. J. Multiphase Flow Vol. 13, No. 2, pp. 199–217, 1987
Printed in Great Britain.

0301-9322/87 $3.00 + 0.00

THE BUBBLE–SLUG FLOW PATTERN TRANSITION AND INSTABILITIES OF VOID FRACTION WAVES

A. MATUSZKIEWICZ,† J. C. FLAMAND and J. A. BOURÉ
Service d'Etudes Thermohydrauliques, Centre d'Etudes Nucléaires de Grenoble, 85 X, 38041 Grenoble, France

(*Received* 7 *March* 1985; *in revised form* 23 *June* 1986)

Abstract—The propagation of spontaneous void fraction disturbances in a nitrogen–water flow has been studied through the statistical analysis of conductivity probe signals, for void fractions ranging from 0.1 to 0.5 and including the bubble–slug transition. The power spectral density function and the standard deviation of the void fraction have been computed for each probe, as well as the system phase factor (related to the wave velocity), the coherence function and the system gain factor between each pair of consecutive probes as functions of frequency. For bubble flow, the results are compatible with the results obtained by other authors. The transition from bubble to slug flow is associated with void fraction wave instabilities. Two kinds of instabilities seem to occur simultaneously: amplitude increase (system gain factor > 1) and wave-breaking.

1. INTRODUCTION

Investigation of propagation phenomena can yield much interesting information on two-phase flows. Interest paid in the past to the so-called void fraction or concentration waves has been renewed recently. These waves are also called continuity or kinematic waves (Wallis 1969) because of the analogy of the simplest equation describing them with the equation of traffic flow waves on a highway analyzed by Lighthill & Whitham (1955).

Void fraction waves were first detected and qualitatively described independently by Zuber (1961) and Wallis (1961). Nassos & Bankoff (1966) carried out a series of experiments on void fraction waves produced by external disturbances. They found that the measured wave velocities are in fair agreement with the continuity wave theory based upon the work of Lighthill & Whitham (1955). A turbulent diffusion process was taken into account to explain the observed decrease in the disturbances (Nassos & Bankoff 1966). For some runs an increase in the disturbance amplitude was observed, and the corresponding diffusion coefficient was negative. Recently, some other studies were carried out on the void fraction waves, mainly in the hope of obtaining some information on the closure law (topological law) for the kinematic model of two-phase flow (Bouré & Mercadier 1981; Bouré 1982). Although this aim is not discussed further here studies in this field give interesting insight into two-phase flow propagation phenomena themselves.

Mercadier (1981) studied, both experimentally and theoretically, the propagation of small spontaneous disturbances (fluctuations) of the void fraction in vertical air–water flows for mean void fractions ranging from 0 to 0.28. His conclusions may be summarized as follows:

—The frequencies of void fraction waves do not exceed a few Hz under his experimental conditions.
—Void fraction waves are not dispersive, i.e. the phase velocity of the waves does not significantly depend on frequency for the observed frequency range.
—The phase velocity of the void fraction waves is always bounded by the velocity of the liquid (lower limit) and by the mean velocity of the gas (upper limit).
—The void fraction waves are damped for bubble flows and the damping decreases as the mean void fraction increases.

†On leave in 1983 from the Institute of Fluid Flow Machinery, Gdansk, Poland.

On the grounds of the last observation, Mercadier (1981) put forward the hypothesis that at some value of the mean void fraction the damping could disappear and that the flow pattern transition (bubble to slug) could be related to the instability of void fraction waves.

The propagation of larger disturbances of void fraction imposed by a special disturbance device was studied by Micaelli (1982) in vertical nitrogen–water co-current flow for mean void fractions ranging from 0 to 0.20. He concluded that at high liquid flow rates ($Re > 6 \cdot 10^4$) the disturbances are strongly damped and the damping could be described by a diffusion law. Moreover, he confirmed that the void fraction waves are not significantly dispersive and that their phase velocity does not depend significantly on the longitudinal position z, at least for mean void fractions < 0.2.

At this point a remark must be made: experimental investigations on void fraction waves are primarily boundary condition problems. (The experimenter has some control on the boundary conditions, such as the flow inlet conditions or at least he can easily measure the inlet disturbance frequency. On the contrary he has practically no control on the detailed structure of the initial conditions, often a so-called "steady" flow which obviously cannot be strictly steady.) Therefore, the experimental disturbance parameters are the frequency and amplitude of the disturbance, and not its wavelength. Accordingly, although the wavelength is definitively a more "fundamental" parameter, most results are expressed hereafter in terms of frequency (this point will be discussed again in section 7.6).

On the basis of a microscopic model for bubble flow and an assumed form of the bubble pair distribution function, Biesheuvel (1983) derived a diffusion-like equation for the void fraction waves of small amplitudes. For negative values of the diffusion coefficient, the waves described by this equation are unstable and the author assumes that this instability is related to a flow pattern transition. The analytical expression of the diffusion coefficient is rather complex and it is difficult to draw any physical conclusion concerning the conditions leading to a flow pattern transition.

In view of our results discussed later, it is worth mentioning some interesting investigations concerning flow pattern transitions. Jones & Zuber (1975) studied experimentally the interrelation between void fraction fluctuations and flow patterns. They found that the probability density function of void fraction fluctuations has maxima at the following void fraction values:

—one near zero for bubble flow;
—one near zero and another near unity for slug or churn flow;
—one near unity for annular flow.

For slug flows, the power spectral density function has a sharp maximum. For a liquid superficial velocity $J_L = 0.15$ m/s, the frequency at which the maximum power spectral density occurred was approximately contained within the range $0.8 < f < 1.6$ Hz for all slug flow runs. According to Tutu (1982, 1984), the investigation of pressure fluctuations can also lead to flow pattern identification. The results of Tutu's work have shown that the probability density function of pressure drop exhibits one or two maxima for bubble or slug (churn) flow, respectively.

Taitel *et al.* (1980) constructed a model based on a physical mechanism to predict flow pattern transitions during steady gas–liquid co-current flow in vertical tubes. They found that at not too large liquid flow rates a steady bubble flow can exist only in tubes which have a diameter larger than some definite value. This value can be predicted by the model. For air–water flows at low pressure, e.g. 10^5 N/m^2, and liquid superficial velocities < 1 m/s, a steady bubble flow could not exist in tubes < 5 cm dia. In such conditions only slug flow could exist. The authors also considered churn flow as an entrance phenomenon, i.e. the early stage of a stable slug flow which exists farther along the tube. Under some conditions the "entrance" region can cover the whole length of the tube.

The main aim of the study presented here is to widen the scope of the works on void fraction waves for mean void fractions > 0.28.

The existence of void fraction waves is considered as being established in the literature cited above. It is also pointed out that the steady-state values of the void fraction for given liquid and gas flow rates (a problem abundantly dealt with in the literature) are not within the scope of this study, although they are given in section 3 for completeness.

To the authors' knowledge, no work has been performed on the propagation of void fraction waves for mean void fractions > 0.28. Thus in the first place, it is necessary to detect them in that

range, and to measure their dispersion, velocity of propagation and attenuation (or amplification). For this purpose the measurements of the coherence function, standard deviation, power spectral density function, system phase and gain factors of the void fraction signals are carried out.

Special emphasis is put on a possible interrelation between an instability of the void fraction waves and the bubble–slug flow pattern transition.

2. EXPERIMENTAL CRITERIA OF WAVE INSTABILITY

The growth of the wave amplitude along the pipe in the direction of its displacement suggests the instability of the wave but this cannot be confirmed experimentally in the strict sense (the growth of amplitude has to be continued indefinitely for the wave to be unstable). The pipe being of finite length, one cannot be quite sure whether the growth of amplitude is related to an instability of the wave or to a long-wave phenomenon. However, another type of instability is known in which the growth of amplitude is continued over a finite distance and during a finite time only. In this type the derivatives of the amplitude become infinite after a finite time, while the amplitude itself remains bounded. An instability of this kind is known as breaking (Whitham 1974).

The simplest equation leading to void fraction waves is of the form (Wallis 1969)

$$\frac{\partial \alpha}{\partial t} + C(\alpha)\frac{\partial \alpha}{\partial z} = 0, \qquad [1]$$

where α is the void fraction and C is the velocity of void fraction waves.

It is possible to demonstrate (Whitham 1974, p. 19) that if at a time $t = 0$ the spatial gradient of the wave velocity is negative then the breaking instability will occur. The point of instability may be found on a characteristic straight line, the slope of which is determined by the initial distribution of wave velocity. The breaking always appears after some delay and at some distance from the point where the gradient was negative at $t = 0$.

The equations of two-phase flows in pipes are generally written as a set of first-order partial differential equations of the form (e.g. Bouré 1980)

$$A_{ij}\frac{\partial u_j}{\partial t} + a_{ij}\frac{\partial u_j}{\partial z} + b_i = 0 \quad i, j = 1, 2, \ldots, n, \qquad [2]$$

where $n = 3$, 5, 7 depending on the utilized model (kinematic, mechanical, thermomechanical, respectively; in all cases, the set [2] includes balance equations and at least one closure equation). The set [2] implies wave phenomena. Depending on the utilized model there are 3, 5 or 7 kinds of waves, but in any case, each model implies at least void fraction waves (Bouré 1982).

Although two-phase flow equations are more complicated than [1], it is assumed further that the conclusions on the instability of waves deduced from [1] are qualitatively valid in the more general case of the set [2]. This would be especially expected in the vicinity of the flow pattern transition where attenuation disappears ($b_i = 0$). In conclusion, the void fraction waves will be experimentally recognized as unstable if amplitude growth and negative wave velocity gradient are simultaneously observed in the pipe.

3. EXPERIMENTS

The OSCAR rig used for the present experiments is a classical low-pressure, nitrogen–water loop already used and described by Micaelli (1982). The test section (figure 1) is vertical (length = 1.75 m) and transparent (Plexiglas). Its 2 × 2 cm cross section is square to facilitate the implementation of 12 conductivity probes (flat walls). The mean void fraction and void fraction fluctuations are measured by processing the signals of these conductivity probes whose electrodes are also square (2 × 2 cm) and mounted flush in two opposite test section walls. The conductivity measured by a probe is thus roughly the conductivity of a cubic volume (2 × 2 × 2 cm) of the two-phase mixture. This volume being sufficiently large, the conductivity is practically unaffected by the behavior of individual bubbles. On the other hand, it is sufficiently small to lead to fairly local quantities (mean void fraction and void fraction fluctuations). The distance between two successive probes is 0.15 m from axis to axis. Twelve probes are installed along the test section

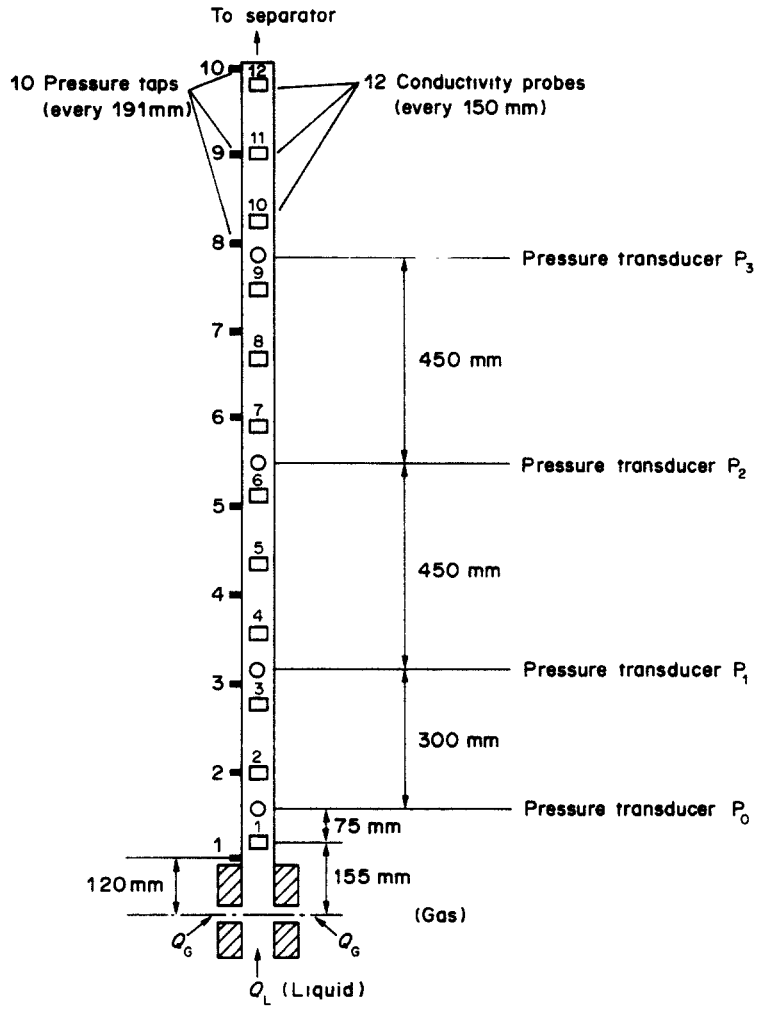

Figure 1. Test section.

(figure 1) but only the signals of eight probes (Nos 4–11) are processed in the present study. The test section is also equipped with 10 pressure taps, which are used to calibrate the conductivity probes as void fraction meters (cf. section 5).

The conductivity probes are supplied with a 10 kHz electrical current and the signal (voltage) is first processed to obtain its mean value and the fluctuations around this mean value. The mean conductivity leads directly to the average void fraction using the calibration curve (details will be given later). The fluctuating part is in turn processed with a computer to obtain:

—for each probe: estimates of the power spectral density function and the standard deviation;
—for each pair of successive probes: estimates of the system phase factor (which leads to the wave velocity), the system gain factor and the coherence function as functions of the frequency.

For the experiments reported here, water and nitrogen flowed co-currently upwards. The separator (a vessel in which the two phases separate and which is located approx. 0.5 m above the test section exit) worked at atmospheric pressure. The water flow rate was kept constant (superficial velocity 0.18 m/s). Such a small water flow rate was useful to control the water temperature (kept at 20°C). On the other hand, a large flow rate could prevent the occurrence of slug flow within the test section. The nitrogen flow rate was adjusted to obtain an average void fraction varying from 0.1 to 0.5 to include the bubble–slug transition. The average void fraction value did not change significantly along the part of the test section under study. The values of mean void fraction

Table 1

	$\bar{\alpha}$									
	0.10	0.15	0.20	0.25	0.30	0.35	0.40	0.45	0.47	0.50
J_G (m/s)	0.04	0.06	0.09	0.13	0.16	0.21	0.27	0.31	0.39	0.42
J_L (m/s)	0.18									

Table 2

	$\hat{\gamma}^2 = 0.35$	$\hat{\gamma}^2 = 0.65$	$\hat{\gamma}^2 = 0.95$
$\epsilon_r(\hat{\gamma}^2)$	21%	8.5%	1%
$\epsilon_r(\hat{H})$	17%	9%	2.8%
$\epsilon_r(\hat{\phi})\cdot\hat{\phi}$	9.7°	5.2°	1.6°

For details see Matuszkiewicz *et al.* (1984).

as a function of gas and liquid superficial velocities corresponding to the flow conditions tested in the present study are given in table 1.

The investigated void fraction fluctuations were those occurring spontaneously in the test section [as in the work by Mercadier (1981), but unlike the investigation of Micaelli (1982)]. They may result in part from the loop, and especially from the injector dynamics, but also probably—see section 7.2—from interactions between bubbles, between bubbles and walls and from turbulence.

More details may be found in former publications: on the rig, in Micaelli (1982); and on this particular series of experiments and on their processing (finite Fourier transform) in Matuszkiewicz *et al.* (1984).

4. STATISTICAL DATA ANALYSIS

Probe signals were processed in order to obtain the power spectral density function, cross-spectral density function, coherence function, system gain and phase factors and standard deviation. These quantities were used in the sense defined by Bendat & Piersol (1971) (see the appendix). To obtain the spectral quantities, the signals were converted from an analog to a digital form and further processed by the fast Fourier transform.

Three requirements were imposed on data acquisition and processing. Statistical errors in spectral quantities have to be as low as possible, and at the same time, as void fraction wave frequencies do not exceed a few Hz, the resolution bandwidth has to be small enough. These are antagonistic requirements and could only be fulfilled if the duration of each single run was sufficiently long. This duration is however, limited by the requirement to maintain constant flow parameters during the run. The choice of the sample record length and of the number of sample records used for statistical averaging was the result of a compromise between these three requirements. Thus, for each run the sample record length and the number of sample records were chosen as $T = 5$ s and $q = 200$, respectively. The resolution bandwidth was thereby $B_e = 0.2$ Hz and the total acquisition time for a single run was about 17 min (statistical errors will be discussed later).

To avoid folding, the sampling frequency has to be at least twice the maximum expected frequency. As the probe signals were filtered by a low-pass filter of 78 Hz maximum frequency† before entering the analyzer, the sampling frequency was chosen as $F_e = 204.8$ Hz. The choice of the sampling frequency and the sample record length imply a number of points of each single sample record $N = F_e T = 1024$. Thus, the elementary frequency increment is $\Delta f = F_e/N = 0.2$ Hz ($\Delta f = B_e$).

Statistical error in spectral quantities mainly depends on the number of sample records used for statistical averaging. In the present studies this number was $q = 200$. The error in power spectral density was 7% and that in the variance was $<0.3\%$. The statistical errors in cross-spectral quantities additionally depend on the actual coherence function values. The statistical errors (ϵ_r) in the coherence function ($\hat{\gamma}^2$), system gain factor ($\hat{H}$) and system phase factor ($\hat{\phi}$) are given in table 2 for some values of the coherence function (for $q = 200$).

†Earlier studies (Mercadier 1981) showed that spontaneous void fraction fluctuations are negligible under equivalent experimental conditions for frequencies >10 Hz. The same observation was made *a posteriori* in the present investigation.

5. CALIBRATION OF THE CONDUCTIVITY PROBES

The electrical conductivity of a two-phase mixture depends on the volume fraction of the gas phase. For a given flow pattern there is a relationship

$$\frac{\bar{k}_\alpha}{k_L} = f(\bar{\alpha}) \qquad [3]$$

between the ratio $\bar{k}_\alpha/k_L$ and the mean void fraction $\bar{\alpha}$, $\bar{k}_\alpha$ being the mean conductivity of the two-phase mixture and k_L the conductivity of the liquid. Many theoretical and experimental studies have been undertaken to establish the relationship between the conductivity of a two-phase mixture and the volume fraction of one of the phases (cf. Turner 1976). These results were obtained with a homogeneous distribution of the dispersed phase. For the case of transition (churn) or slug flow, the gas phase is not uniformly distributed, and the above results are not applicable. Thus, in order to find the explicit form of [3] a method of calibration has been used.

To calibrate the conductivity probes it is necessary to measure the conductivity of the liquid and of the mixture and at the same time to measure the mean void fraction. It was verified experimentally that, within the range of parameters covered in the experiments, the conductivity of the mixture did not visibly vary along the test section. This implies that the mean void fraction is nearly constant along the test section. Moreover, as the liquid flow rate was small ($J_L = 0.18$ m/s), the pressure drop due to friction was small, and it was possible to employ a manometric method (Mercadier 1981)† to measure the mean void fraction. A large number of runs were done to check whether an explicit form of [3] obtained with the aid of calibration is affected by water impurities, temperature and location of probe. The ratio $\bar{k}_\alpha/k_L$ does not depend on these factors, as can be seen in figure 6 where the points from different tests are marked. The result of a regression analysis is very well approximated by a second-order polynomial:

$$\frac{\bar{k}_\alpha}{k_L} = a_0 + a_1\bar{\alpha} + a_2\bar{\alpha}^2, \qquad [4]$$

where the coefficients

$$a_0 = 0.999, \quad a_1 = -1.363 \quad \text{and} \quad a_2 = 0.212$$

are approximated for practical use by

$$a_0 = 1.00, \quad a_1 = -1.36 \quad \text{and} \quad a_2 = 0.21. \qquad [5]$$

The correlation coefficient is $r^2 = 1.00$ and the standard deviations of the exact polynominal coefficients are, respectively,

$$\sigma(a_0) = 0.0006, \quad \sigma(a_1) = 0.0088 \quad \text{and} \quad \sigma(a_2) = 0.0188.$$

Knowing the value of the ratio $\bar{k}_\alpha/k_L$ [4] yields the value of the mean void fraction. As the normalized standard error in $(\bar{k}_\alpha/k_L)$ was $<3\%$ for all runs, the corresponding normalized error in the mean void fraction was $<5\%$.

6. STANDARD DEVIATION OF THE VOID FRACTION

The evolution of the standard deviation of the void fraction can yield much interesting information on the development of two-phase flows. If [4] is assumed to hold for the instantaneous values of the void fraction, it is possible to calculate the variance of the void fraction from conductivity signals. The void fraction and the conductivity of the mixture may be decomposed

†If the liquid flow rare is zero the momentum balance equation of a two-phase mixture can be simplified to the form

$$dP/dz = -g\rho_L(1-\bar{\alpha}),$$

P being the pressure, g the acceleration of gravity and ρ_L the density of the liquid phase. Thus, measurement of the pressure drop can supply the value of the mean void fraction.

into sums of two terms, i.e.

$$\alpha = \bar{\alpha} + \alpha' \qquad [6]$$

and

$$k_\alpha = \bar{k}_\alpha + k'_\alpha, \qquad [7]$$

where overbar and prime denote mean and fluctuation terms, respectively. Relation [3] can then be expressed in the following way:

$$\frac{\bar{k}_\alpha}{k_L} + \frac{k'_\alpha}{k_L} = f(\bar{\alpha}) + \alpha' \left.\frac{df}{d\alpha}\right|_{\alpha = \bar{\alpha} + \eta\alpha'} \quad 0 \leqslant \eta \leqslant 1; \qquad [8]$$

[4] and [5] lead to the following linear relationship:

$$\frac{df}{d\alpha} = -1.36 + 0.42\,\bar{\alpha}. \qquad [9]$$

It will be seen later that the standard deviation of the void fraction, which is a measure of the order of magnitude of α', varies (cf. figure 7) from 0.012 for low $\bar{\alpha}$ to 0.08 for $\bar{\alpha} \simeq 0.38$. In the unfavorable case where α fluctuates between $0.38 - 0.08 = 0.30$ and $0.38 + 0.08 = 0.46$, [9] yields

$$-1.23 \leqslant \frac{df}{d\alpha} \leqslant -1.17$$

or

$$\frac{df}{d\alpha} = 1.2 \pm 2.5\% = \left.\frac{df}{d\alpha}\right|_{\alpha = \bar{\alpha}} \pm 2.5\%.$$

Thus, it is possible to let $\eta = 0$ and to obtain from [3] and [8] the relationship

$$\frac{k'_\alpha}{k_L} \simeq \alpha' \left.\frac{df}{d\alpha}\right|_{\alpha = \bar{\alpha}}. \qquad [10]$$

From [10] it is possible to express the variance or standard deviation of the void fraction through the variance of the conductivity probe signal:

$$\bar{\Psi}^2_{k'_\alpha} = \frac{1}{Tq} \sum_{n,i} (k'_\alpha)^2_{n,i}, \qquad [11]$$

k'_α being the conductivity probe signal and summations of n and i denoting time and statistical averagings, respectively. Thus, the standard deviation of void fraction can be expressed in the following form:

$$\sigma_\alpha = \sqrt{\langle \overline{\alpha'^2} \rangle} = \frac{1}{1.36 - 0.42\bar{\alpha}} \frac{1}{k_L} \sqrt{\bar{\Psi}^2_{k'_\alpha}}. \qquad [12]$$

7. RESULTS AND DISCUSSION

7.1. Preliminary observations

The mean void fractions investigated in the experiments span the range $0.1 \leqslant \bar{\alpha} \leqslant 0.5$. Some signals and power spectral density functions, one for each value of the void fraction, are shown in figures 2–4. The figures were drawn by a plotter and the scales were chosen by the computer to be as large as possible. They are therefore not the same in the different figures. The discrete points ($\Delta f = 0.2$ Hz, $\Delta t = 4.88$ ms), which are the results of sampling, are joined by straight-line segments. Qualitatively, the observed flow pattern may be classified as follows:

bubble flow for: $\bar{\alpha} = 0.10, 0.15, 0.20, 0.25$
transition flow (churn) for: $\bar{\alpha} = 0.30, 0.35, 0.40, 0.45$
slug flow for: $\bar{\alpha} = 0.47, 0.50$.

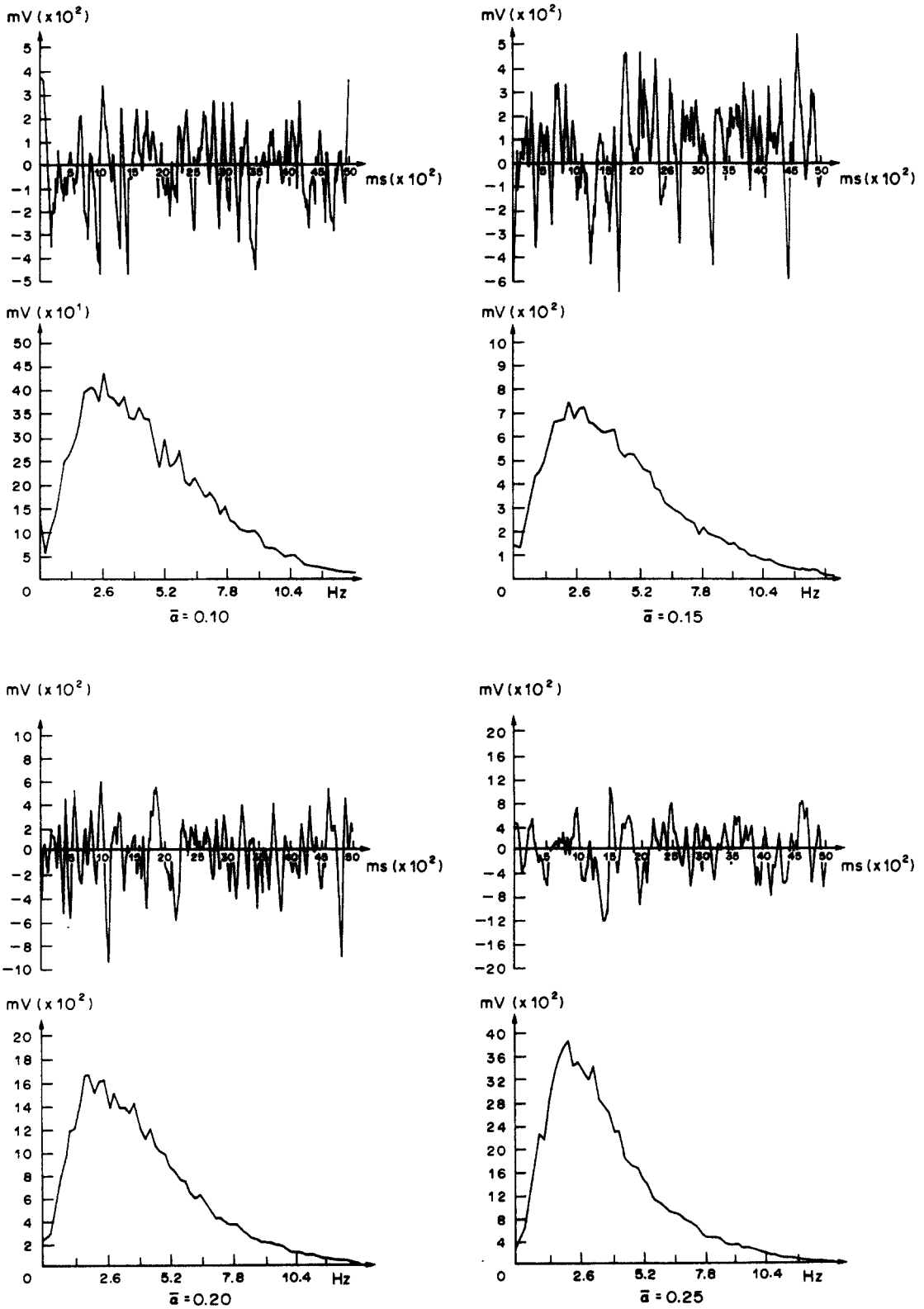

Figure 2. Typical signals and power spectral density functions, probe 11 (signal coordinates in arbitrary units).

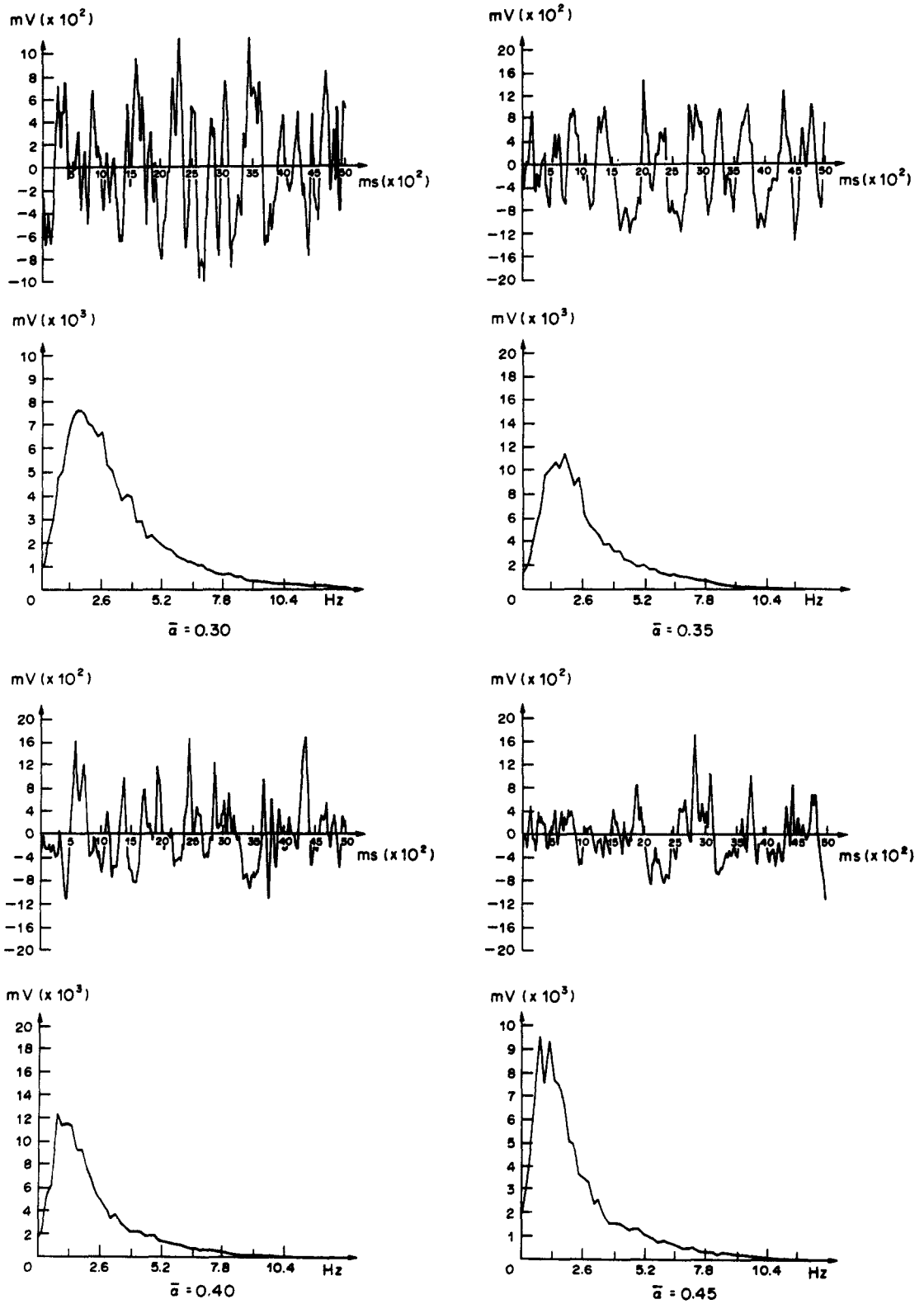

Figure 3. Typical signals and power spectral density functions, probe 11 (signal coordinates in arbitrary units).

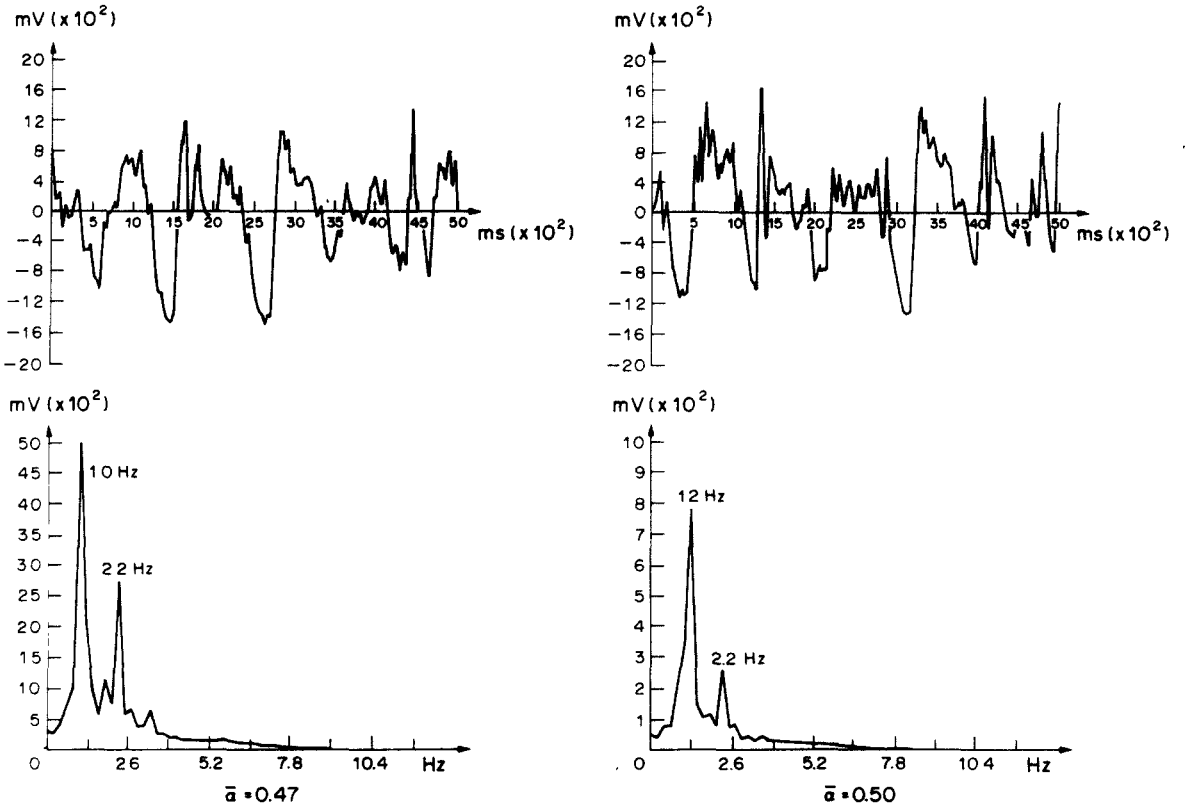

Figure 4. Typical signals and power spectral density functions, probe 11 (signal coordinates in arbitrary units).

The liquid flow rate being small, the visual observation can be accepted as a criterion for flow pattern identification.

Bubble flow was observed for $\bar{\alpha} \leqslant 0.25$, no Taylor bubble appearing along the test section of 1.8 m. This observation contradicts the prediction of a model proposed by Taitel *et al.* (1980) that no bubble flow could exist in tubes < 5 cm dia (here the cross section is a 2×2 cm^2). It is possible, however, that the test section in our experiments was too short to enable Taylor bubbles to develop. Some results of this work support such a possibility. On the other hand, our observations confirm those of Taitel *et al.* (1980) that churn flow is an entrance phenomenon, i.e. the early stage of a stable slug flow which exists farther along the tube. The tests for bubble flow confirmed Mercadier's results (1981) in that the spontaneous disturbances of void fraction are limited to a range of a few Hz, and the void fraction waves are not amplified. However, they appear as slightly dispersive, at least at low frequencies, even for small void fractions as will be seen later (sections 7.4 and 7.5).

Slugs, arising in the upper part of the test section, were observed only for $\bar{\alpha} = 0.47$ and $\bar{\alpha} = 0.50$. For these void fraction values, the power spectral density functions show very sharp peaks for the frequencies $f = 1.0$ and 1.2 Hz respectively, as can be seen in figure 4 (it is necessary to recall here that the minimum recognizable frequency increment is 0.2 Hz). This is in excellent agreement with the results obtained by Jones & Zuber (1975). They found that the characteristic slug frequency (i.e. the frequency corresponding to a sharp maximum of the power spectral density function) is limited to the range $0.8 < f < 1.0$ Hz for $\bar{\alpha} = 0.48$ and $J_L = 0.15$ m/s, which is very close to the result of the present work: $f = 1.0$ Hz for $\bar{\alpha} = 0.47$ and $J_L = 0.18$ m/s.

Finally, as discussed in Bouré & Matuszkiewicz (1984)—see also figure 7 hereafter—the signals delivered by probes 6 and 10 were probably subject to systematic bias. To avert the consequences of such bias, the results for wave velocities and system gain factors presented here (sections 7.4 and 7.5, and figures 8, 9 and 11) are not given for the probe pairs 5–6, 6–7, 9–10 and 10–11. They involve instead the relevant averages between probes 5 and 7 and between probes 9 and 11.

7.2. Standard deviation

In figure 5 an example of the spatial evolution of the signals taken at different longitudinal positions along the test section is presented. It can be easily seen that the amplitude of the fluctuations increases with the longitudinal position of the probe. The mean void fraction being constant along the test section, an investigation of the spectral distribution of the standard deviation of void fraction can yield some interesting information on bubble and churn flows ($0.10 \leqslant \bar{\alpha} \leqslant 0.45$). The standard deviation of void fraction deduced from the standard deviation of the signal itself (cf. [12]) is given in figure 7. There are no points corresponding to $\bar{\alpha} = 0.47$ and $\bar{\alpha} = 0.50$ in figure 7. The values of the standard deviation of void fraction for $\bar{\alpha} = 0.47$ are on average 2.3 times greater than those for $\bar{\alpha} = 0.45$ and the values of the standard deviation of void for $\bar{\alpha} = 0.50$ are on average 2.8 times greater than those for $\bar{\alpha} = 0.45$. Exact values of the standard deviation of void fraction for $\bar{\alpha} = 0.47$ and $\bar{\alpha} = 0.50$ are not significant because they can be affected by a large bias error due to the presence of a sharp maximum in the power spectral density function (figure 4). Two observations can be easily drawn from figure 7.

Firstly, for a given $\bar{\alpha}$, the standard deviation of void fraction increases with the probe number, i.e. with the longitudinal position of the probe. This may be due to an instability of void fraction waves, which at low values of $\bar{\alpha}$ would be contradictory to the results presented below (section 7.4) for the system gain factor, as well as to Mercadier's (1981) results. This may also be due to new fluctuations arising between each pair of probes as already discussed at the end of section 3. The discussion will be continued in the following sections.

Secondly, at a given location, the standard deviation of void fraction goes through a maximum as $\bar{\alpha}$ increases, and the larger the distance from the inlet, the more pronounced the maximum. The value $\bar{\alpha}_\sigma$ corresponding to the maximum decreases very slightly with z, from $\bar{\alpha}_\sigma \simeq 0.38$ at probe 4 to $\bar{\alpha}_\sigma \simeq 0.36$ at probe 11. It is possible that, around $\bar{\alpha}_\sigma$, a void fraction wave instability is superimposed on new fluctuations arising, which may ultimately lead to the bubble–slug transition in long pipes.

7.3. Coherence function between successive probes

One of the most striking results of the data processing is a drastic change in coherence function (γ^2) values between the signals obtained for $\bar{\alpha} \leqslant 0.45$ and those obtained for $\bar{\alpha} = 0.47$ and $\bar{\alpha} = 0.50$.

For $0.10 \leqslant \bar{\alpha} \leqslant 0.45$, the greatest mean value $\overline{\gamma^2}$ (calculated with the seven pairs of probes) of γ^2 varies irregularly between 0.49 and 0.59, the largest individual value being 0.68. The signals of successive probes are only weakly correlated, which corroborates the assumption made above (section 7.2) that new fluctuations arise between probes. Except in a few particular cases, in which the values of γ^2 for probes 4–5 and/or 5–6 are <0.4, γ^2 does not vary significantly with z.

On the contrary, for $\bar{\alpha} = 0.47$ and $\bar{\alpha} = 0.50$, the greatest mean values of $\overline{\gamma^2}$ are respectively 0.91 and 0.93, denoting very well correlated signals, at least at some particular frequencies (respectively, 1 and 1.2 Hz). For these frequencies γ^2 does not vary significantly with z (the lowest individual value being 0.90) which means that it does not seem to depend on the actual presence of slugs since these appear only in the upper part of the test section. For the other frequencies, γ^2 may vary significantly with z.

Clearly, an important transition occurs between $\bar{\alpha} = 0.45$ and $\bar{\alpha} = 0.47$ and it corresponds visually to the appearance of slugs.

7.4. System gain factor

For $0.10 \leqslant \bar{\alpha} \leqslant 0.45$, the geometric mean $\bar{H}$ (calculated with the seven pairs of probes) of the system gain factor varies very slightly with the void fraction and the frequency at least for low frequencies ($f < 2$ Hz). For $\bar{\alpha} = 0.47$ and $\bar{\alpha} = 0.50$, $\bar{H}$ varies relatively more with the frequency but the variations remain small. The values close to the maximum $\bar{H}_{max}$ of $\bar{H}$ as a function of $\bar{\alpha}$ are given in figure 10, together with the corresponding frequencies. As for $\overline{\gamma^2}$ (section 7.3), there is drastic change in $\bar{H}_{max}$ between $\bar{\alpha} = 0.45$ ($\bar{H}_{max} < 1$) and $\bar{\alpha} = 0.47$ ($\bar{H}_{max} > 1$). As mentioned in section 7.3, an important transition occurs between $\bar{\alpha} = 0.45$ and $\bar{\alpha} = 0.47$.

For $0.10 \leqslant \bar{\alpha} \leqslant 0.45$ the void fraction waves are attenuated, which confirms Mercadier's (1981) results. At first glance it could be interpreted as a contradiction to measure a system gain factor <1 (figure 10), and a standard deviation of void fraction increasing with the longitudinal position

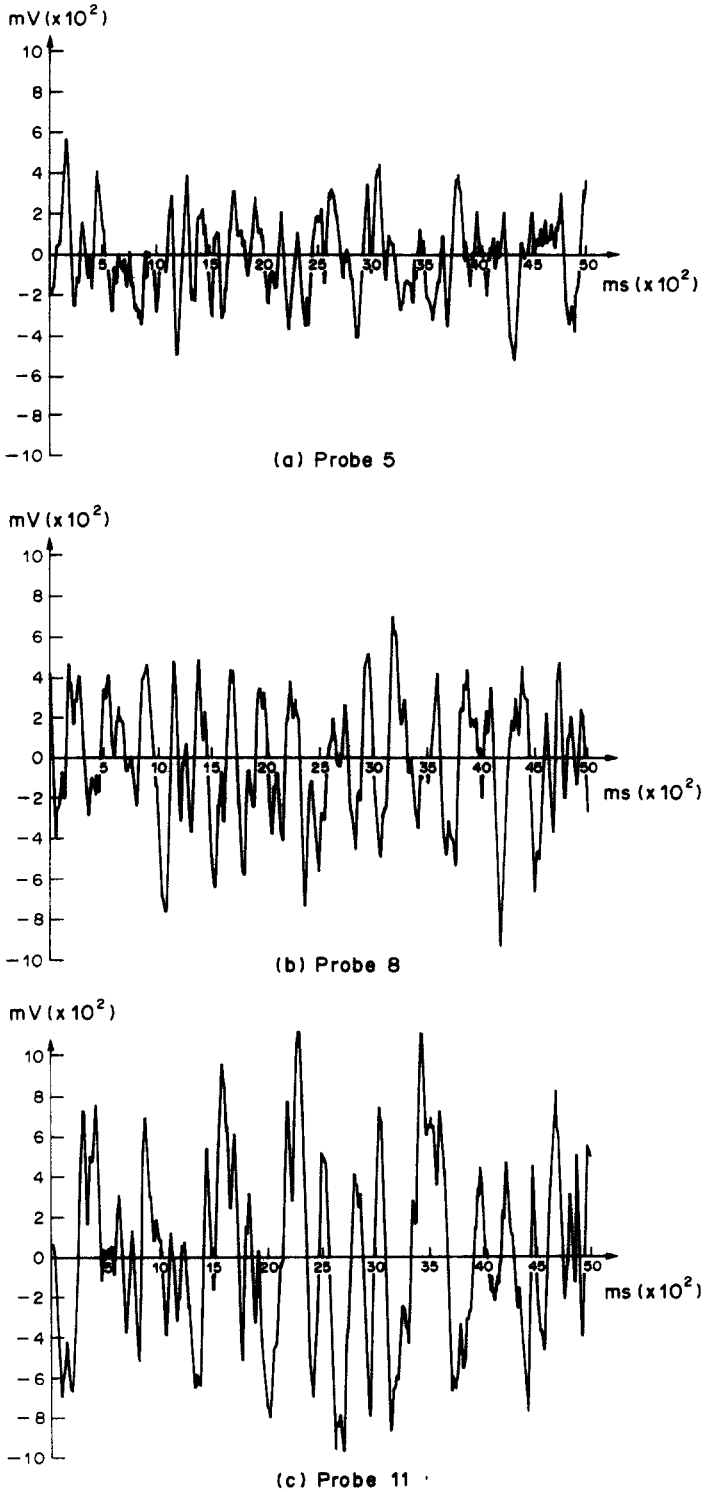

Figure 5. Spatial evolution of the signal for $\bar{\alpha} = 0.30$.

of the probe (figure 7). However, it is worth recalling that on the one hand the standard deviation is a measure of the mean amplitude of the fluctuations recorded by one probe, while on the other hand the system gain factor is a measure of the growth of the *coherent part of signals* recorded by two probes (Bendat & Piersol 1971, p. 338). Thus, the standard deviation of void fraction increases with the longitudinal position of the probe because of new fluctuations arising between two successive probes while the system gain factor is < 1 because the void fraction waves are

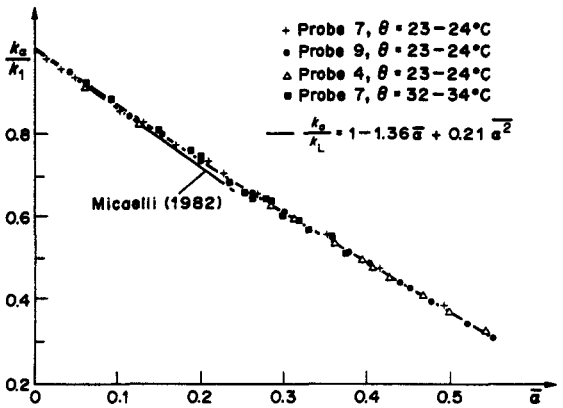

Figure 6. Conductivity probe calibration curve.

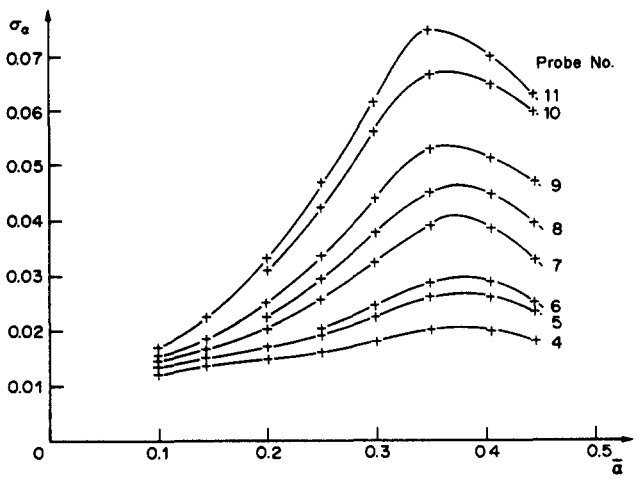

Figure 7. Standard deviation of the void fraction.

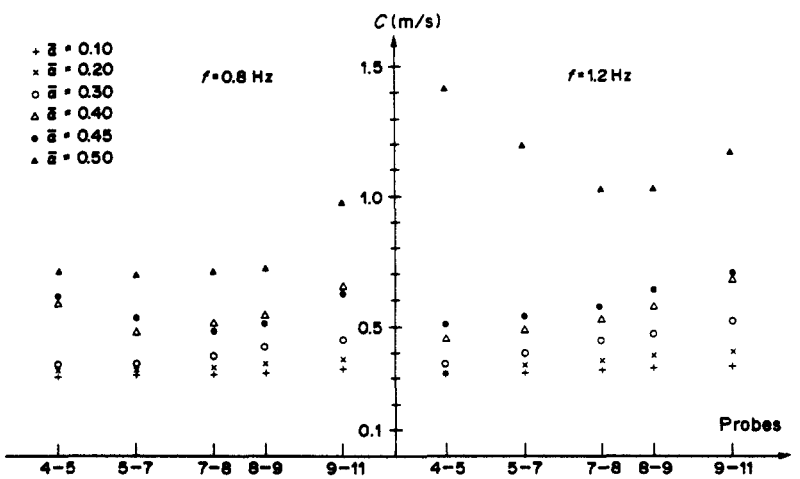

Figure 8. Spatial distribution of the velocity of void fraction waves.

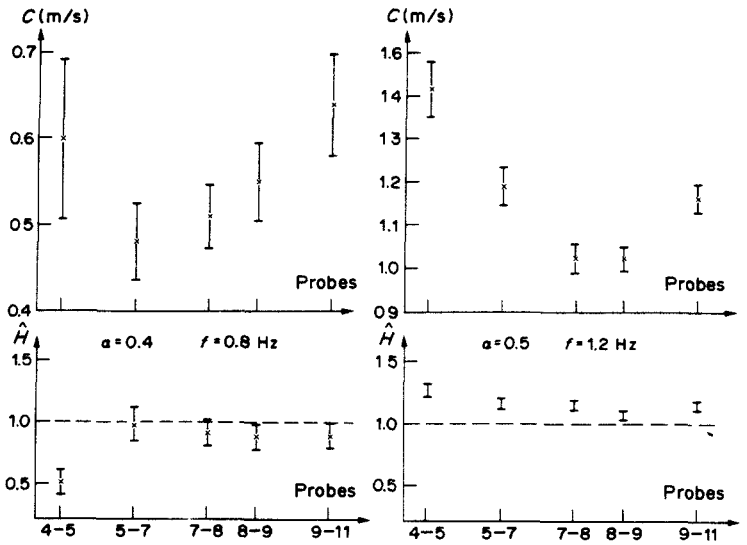

Figure 9. Spatial distribution of the gain and of the velocity of void fraction waves.

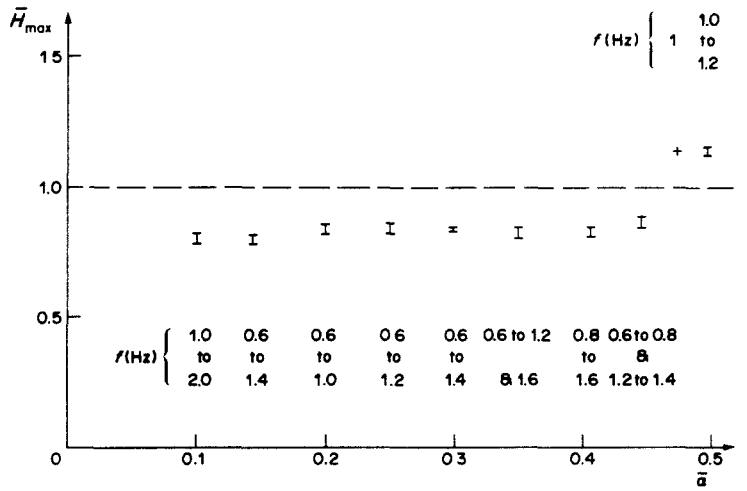

Figure 10. Maximum mean gain factor as a function of the void fraction.

damped. Again this corroborates the assumption made in section 7.2 on the origin of the standard deviation increase with z.

7.5. Wave velocity

Measurements of the system phase factor between each pair of successive probes (distance d) enable the calculation of void fraction wave velocities in the following way:

$$C = \frac{2\pi f d}{\hat{\Phi}},$$

where $\hat{\Phi}$ is an estimate of the system phase factor. The results show that for a given value of $\bar{\alpha}$, the wave velocity depends on the longitudinal position even for bubble flows, which differs from Mercadier's (1981) results, and on the frequency, particularly for $\bar{\alpha} = 0.47$ and $\bar{\alpha} = 0.50$, i.e. for slug flows. In the present study the propagation velocity calculated between probes 9 and 11 was, for $\bar{\alpha} \leqslant 0.45$, always higher than that calculated between probes 4 and 5 (see figure 8). The difference goes through a maximum when α increases, varying from a few % at low $\bar{\alpha}$ to $>50\%$.

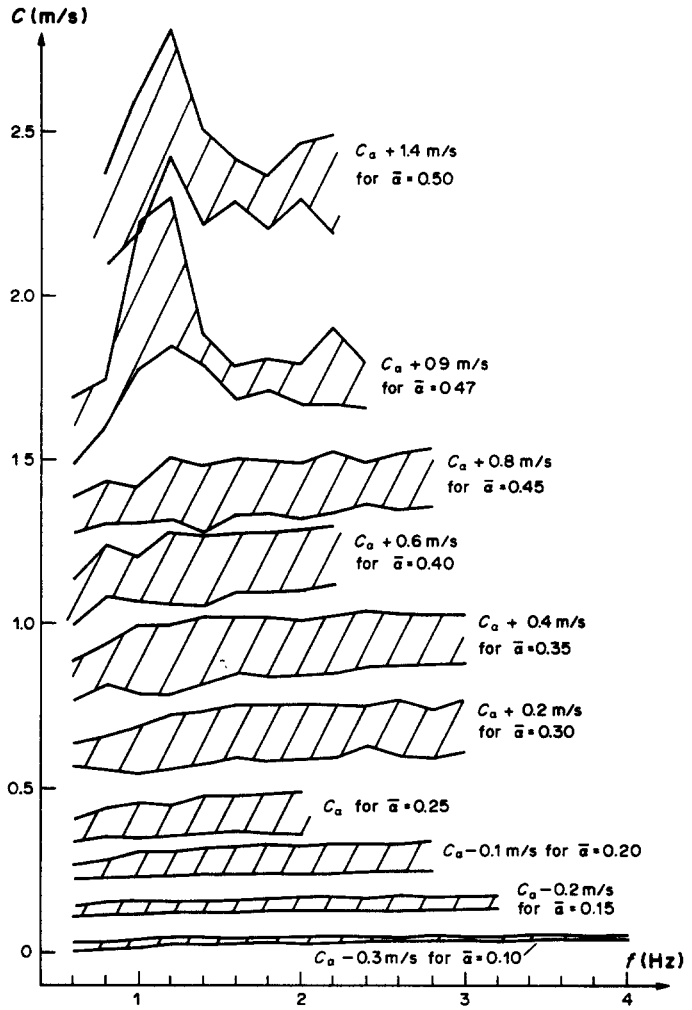

Figure 11. Influence of the frequency on the velocity of void fraction waves.

The relative differences of pressure and propagation velocity of void fraction waves between probes 4–5 and 9–11 for the frequency $f = 1.2$ Hz are given in table 3.

Under the experimental conditions of the present study the void fraction is practically constant along the test section. As ρ_G (density of gas phase) $\sim P$, the mass-balance equation of the gas phase leads to

$$\frac{\Delta P}{P} + \frac{\Delta W_G}{W_G} + \frac{\Delta \bar{\alpha}}{\bar{\alpha}} = 0$$

(W_G being the velocity of the gas phase), and it implies that the relative difference of gas velocity is of the same order of magnitude as the relative difference of pressure. Thus, it can be noted (cf. table 3) that the relative difference of the propagation velocity of void fraction waves is markedly greater than the relative difference of the mean gas velocity. This provides experimental verification of the assumption that apart from the average motion of gas there is another cause of the propagation of void fraction waves.

Table 3

	$\bar{\alpha}$							
	0.10	0.15	0.20	0.25	0.30	0.35	0.40	0.45
$-\Delta P/P$	0.067	0.064	0.060	0.057	0.054	0.050	0.047	0.044
$\Delta C/C$	0.071	0.11	0.22	0.26	0.46	0.55	0.49	0.37

For void fractions $\bar{\alpha} \geqslant 0.35$ and frequencies close to the characteristic slug frequency the spatial distribution of the wave velocity is well-marked. It is very interesting to compare it with the spatial distribution of the system gain factor (figure 9). In figure 9 (left-hand part) distributions are shown for a void fraction $\bar{\alpha} = 0.40$ (distribution for $\bar{\alpha} = 0.45$ and to a lesser extent for $\bar{\alpha} = 0.35$ are quite similar) and for the frequency $f = 0.8$ Hz, which is close to the characteristic slug frequency (cf. figure 4). Between probes 5 and 7, the propagation velocity of void fraction waves attains a minimum and the system gain factor is very close to 1. This observation was made for the frequency $f = 0.8$ Hz. In figure 8 are also shown spatial distributions of wave velocities for another frequency, $f = 1.2$ Hz: for $\bar{\alpha} \leqslant 0.45$, the spatial distribution of the wave velocity does not show any minimum, and the system gain factor always remains < 1.

Slugs were not observed in the test section for $\bar{\alpha} \leqslant 0.45$. This could be due to the damping which prevails along the test section ($H < 1$ for successive pairs of probes) or to the fact that the test section is not sufficiently long for the development of slugs. For void fractions $\bar{\alpha} = 0.47$ and $\bar{\alpha} = 0.50$, slugs effectively arise in the upper part of the test section.

In figure 9 (right-hand part) the spatial distributions of the wave velocity and of the system gain factor are shown for $\bar{\alpha} = 0.50$ and for the frequency $f = 1.2$ Hz corresponding to the sharp peak of the power spectral density function (see figure 4). The distributions for $\bar{\alpha} = 0.47$ are quite similar but the characteristic slug frequency is then $f = 1.0$ Hz. Under these conditions the spatial distribution of the wave velocity clearly shows a minimum. The system gain factor is markedly > 1 for all points. The appearance of slugs is then accompanied by two characteristics of instability, i.e. system gain factor > 1 and negative spatial gradient of wave velocity. The instability of the void fraction waves also appears for a certain frequency.

For bubble and churn flows, i.e. $\bar{\alpha} \leqslant 0.45$, the void fraction waves are only slightly dispersive. On the contrary, for slug flow, i.e. for $\bar{\alpha} = 0.47$ and $\bar{\alpha} = 0.50$, the wave velocity depends very much on the frequency. In figure 11 the wave velocity range along the test section is shown, for each value of $\bar{\alpha}$, as a function of the frequency. For slug flow the wave velocity goes through a maximum for $f \simeq = 1.2$ Hz, i.e. the frequency corresponding to the sharp peak of the power spectral density function for $\bar{\alpha} = 0.50$.

7.6. Wavelength

The wavelength being an invariant of reference it would appear as more rational to express all experimental results as functions of the wavelength rather than of the frequency. In practice it is an impossible or at least a very difficult task. For the sake of completeness the orders of magnitude of the wavelengths can be calculated using the formula $\lambda = C/f$. It should be noted, however, that the wavelengths obtained in this way are subject to large errors. The relative error on frequency (frequencies of interest being of the order of 1 Hz) and the relative error on wave velocity (in the most unfavorable case) being 20%, the relative error on wavelength can attain as much as 40%. Then only the order of magnitude is significant for the calculated values. The wavelength of the void fraction waves increases from about 0.3 m for bubble flow to about 0.9 m for slug flow. The wavelength for slug flow is obviously greater than typical Taylor bubble length, because it includes both the length of a Taylor bubble and the length of the plug separating two successive Taylor bubbles.

8. CONCLUSIONS

The propagation of the void fluctuation disturbances occurring spontaneously in an upward vertical, nitrogen–water flow has been studied at atmospheric pressure, through statistical analysis of the signals of eight conductivity probes and for a single small liquid flow rate ($J_L = 0.18$ m/s), but using a void fraction range including the bubble–slug transition ($0.1 \leqslant \bar{\alpha} \leqslant 0.5$).

The results for bubble flow are in agreement with the results obtained in the past. The spectrum of natural disturbances is narrow, i.e. its upper limit does not exceed a few Hz.† The disturbances

†This is well below the limit defined by the dimensions of the probe (2 × 2 cm). It is not possible to detect waves whose wavelength is of the order of $\leqslant 0.02$ m, i.e. waves, for which $f > C_{min}/0.02$. Thus, the waves which are to be recorded must have frequencies $f < 15.4$ Hz for bubble flow and $f < 35$ Hz for slug flow. These conditions are well-fulfilled as can be seen in the plots of the power spectral density functions (figures 2–4).

propagate at a velocity different from the velocities of the gas and of the liquid. This velocity is nearly independent of the frequency. The spatial variation of the wave velocity is significantly larger than the increase of the mean gas velocity.

The analysis of the standard deviation of void fraction, system gain factor and coherence function, suggests that sources of void fraction fluctuations are distributed all along the tube. These sources are likely to be interactions between bubbles, between bubbles and the walls, and turbulence. Fluctuations arise at any cross section and are superimposed upon the fluctuations arriving there by propagation.

Void fraction waves are slightly dispersive, the dependency of C on the longitudinal position and on the frequency increasing as $\bar{\alpha}$ increases, from practically zero to a significant dependency.

The results corresponding to churn and slug flows are compatible with the hypothesis relating the appearance of slugs to the instability of void fraction waves.

For $0.35 \leqslant \bar{\alpha} \leqslant 0.45$ a smooth transition occurs. The standard deviation of the void fraction begins to decrease. The disturbances are damped or amplified as they propagate (the system gain factor H is not known with sufficient accuracy to draw conclusions) but, in most cases, very slightly. Around $f = 0.8$ Hz the wave velocity goes through a well-marked minimum (see figure 9). It is probable that the test section was too short for slugs to develop.

For $\bar{\alpha} \geqslant 0.45$, a sharper transition occurs. The coherence function of successive probe signals increases abruptly for some "sensitive" frequencies (from $\overline{\gamma^2} \simeq 0.55$ to $\overline{\gamma^2} > 0.90$ for $f = 1.0$ Hz and $\bar{\alpha} = 0.47$ or for $f = 1.2$ Hz and $\bar{\alpha} = 0.50$) which are close to the above-mentioned frequency $f = 0.8$ Hz. Simultaneously, for the sensitive frequencies the power spectral density function has a sharp peak, the system gain factor becomes > 1, the wave velocity goes through a maximum (figure 11) and the spatial distribution of the wave velocity has a well-marked minimum (figure 9). The corresponding void fraction waves are definitely unstable. Slugs are actually observed in the upper part of the test section. One can also tentatively conclude that the frequency relevant to the instability of the void fraction waves and the flow pattern transition is an increasing function of the mean void fraction ($f = 1.0$ Hz for $\bar{\alpha} = 0.47$ and $f = 1.2$ Hz for $\bar{\alpha} = 0.50$). However, it is recalled that the minimum recognizable frequency increment is $\Delta f = 0.2$ Hz.

Finally, the actual appearance of slugs results from the development of a weak instability, and entails a transition length (the larger the average void fraction, the stronger the instability) which cannot be predicted with the present knowledge in this field. The actual bubble–slug transition is closely related to the occurrence of sharp peaks in the power spectral density function and may be characterized by a sudden increase in the coherence function of natural fluctuations at two successive probes for some "sensitive" frequencies.

Obviously, the results of the present study raise many questions which remain to be answered, but the existence of a relationship between the bubble–slug transition and the void fraction wave instability has been substantiated.

REFERENCES

BENDAT, J. S. & PIERSOL, A. G. 1971 *Random Data: Analysis and Measurement Procedures.* Wiley-Interscience, New York.

BIESHEUVEL, A. 1983 On concentration waves in bubbly liquids. Presented at *Euromech Colloquium 176*, Grenoble, France, 21–23 Sept.

BOURÉ, J. A. 1980 Multiphase flow modeling, I. Fundamentals; II. Development of practical models. Presented at *Semin. on Multiphase Processes in LMFBR Safety Analysis*, Ispra, Italy, May.

BOURÉ, J. A. 1982 Kinematic models, void fraction waves and other propagation phenomena in two phase flows. In *Proc. 9th U.S. National Congr. of Applied Mechanics* (Edited by PAO, Y. H.; Comm. Chairman), pp. 85–92. ASME, New York.

BOURÉ, J. A. & MATUSZKIEWICZ, A. 1984 Stability of void fraction waves and bubble slug transition. Presented at *European Two-phase Flow Group Mtg*, Rome, Italy.

BOURÉ, J. A. & MERCADIER, Y. 1982 Existence and properties of flow structure ways in two-phase bubbly flows. In *Proc. IUTAM Symp.*, Pasadena, Calif. June 1981; *Appl. scient. Res.* **38**, 297–303.

JONES, O. C. JR & ZUBER, N. 1975 The interrelation between void fraction fluctuations and flow pattern in two phase flow. *Int. J. Multiphase Flow* **2**, 273–306.

LIGHTHILL, M. J. & WHITHAM, G. B. On kinematic waves. *Proc. R. Soc.* **A229**, 281–316.

MATUSZKIEWICZ, A., FLAMAND, J. C. & BOURÉ, J. A. 1984 Stabilité des ondes de taux de vide et transition écoulement à bulles—écoulement à bouchons. Rapport CEA-R-5274.

MERCADIER, Y. 1981 Contribution à l'étude des propagations de perturbations de taux de vide dans les écoulements diphasiques eau–air à bulles. Thèse, Université Scientifique et Médicale et Institut National Polytechnique de Grenoble, France.

MICAELLI, J. C. 1982 Propagation d'ondes dans les écoulements diphasiques à bulles à deux constituants. Etude théorique et expérimentale. Thèse, Université Scientifique et Médicale et Institut National Polytechnique de Grenoble, France.

NASSOS, G. P. & BANKOFF, S. G. 1966 Propagation of density disturbances in an air–water flow. In *Proc. 3rd Int. Conf. on Heat Transfer*, Vol. IV, pp. 234–246. AIChE, New York.

TAITEL, Y., BARNEA, D. & DUKLER, A. E. 1980 Modeling flow pattern transitions for steady upward gas–liquid flow in vertical tubes. *AIChE Jl* **26**, 345–354.

TURNER, J. C. R. 1976 Two-phase conductivity. The electrical conductance of liquid–fluidized beds of spheres. *Chem. Engng Sci.* **31**, 487–492.

TUTU, N. K. 1982 Pressure fluctuations and flow pattern recogntion in vertical two phase gas–liquid flows. *J. Multiphase Flow* **8**, 443–447.

TUTU, N. K. 1984 Pressure drop fluctuations and bubble–slug transition in a vertical two-phase air–water flow. *Int. J. Multiphase Flow* **10**, 211–216.

WALLIS, G. B. 1961 Two-phase flow phenomena associated with the boiling of liquids. Ph.D. Thesis, Cambridge Univ., Cambs.

WALLIS, G. B. 1969 *One-dimensional Two-phase Flow*. McGraw-Hill, New York.

WHITHAM, G. B. 1974 *Linear and Nonlinear Waves*. Wiley, New York.

ZUBER, N. 1961 Steady state, transient respnse, operating limits and continuity waves in two-phase flow systems. General Electric Report 61GL215.

APPENDIX

Basic Definitions of the Statistical Functions used (from Bendat & Piersol 1971)

The conductivity signal $x(t)$ has been digitized every $\Delta t = T/N$, where T is the duration of a single sample record and N is the number of points recorded for one sample (here $T = 5$ s, $N = 1024$). Then, the discrete approximation of the finite Fourier transform has been used in the following form:

$$x(f_K) = \Delta t \sum_{n=0}^{N-1} x_n \exp(-2\pi jfn\,\Delta t), \qquad [A.1]$$

where

$$j = \sqrt{-1},$$

$$x_n = x(n \cdot \Delta t) \qquad [A.2]$$

and

$$f_K = \frac{K}{N \cdot \Delta t} = \frac{K}{T}, \quad K = 0, 1, \ldots, N-1. \qquad [A.3]$$

The estimate of the power spectral density function for the ith sample has been expressed as follows:

$$\tilde{G}_{x,i}(f_K) = \frac{2}{N \cdot \Delta t} |X_i(f_K)|^2, \quad i = 1, 2, \ldots, q. \qquad [A.4]$$

To obtain the final estimate of the power spectral density function, $\tilde{G}_x(f_K)$, for one run, statistical averaging has been performed on $q = 200$ samples, i.e.

$$\tilde{G}_x(f_K) = \frac{1}{q} \sum_{i=1}^{q} \tilde{G}_x(f_K). \qquad [A.5]$$

The estimate of the standard deviation of the conductivity signal

$$\hat{\Psi}_x^2 = \frac{1}{N \cdot \Delta t} \sum_{n=0}^{N-1} \left\{ \frac{1}{q} \sum_{i=1}^{q} x_{n,i}^2 \right\} \qquad [A.6]$$

has been calculated in the following way:

$$\hat{\Psi}_x^2 = \frac{1}{N \cdot \Delta t} \sum_{K=0}^{N-1} \hat{G}_x(f_K). \qquad [A.7]$$

Formula [A.7] is an approximation of the exact relation

$$\Psi_x^2 = \int_0^\infty G_x(f)\, df \qquad [A.8]$$

between the power spectral density function, $G_x(f)$, and the standard deviation, Ψ_x^2 (Bendat & Piersol 1971, p. 86).

Two signals $x_i(t)$ and $y_i(t)$, from different probes, have to be processed in order to obtain estimates of the coherence function, and the system gain and phase factors. These functions are expressed in terms of the cross-spectral density function. The estimate of the cross-spectral density function for the ith sample has been calculated as follows:

$$\tilde{G}_{xy,i}(f_K) = \frac{2}{N \cdot \Delta t} X_i^*(f_K) \cdot Y_i(f_K), \qquad [A.9]$$

where $X_i^*(f_K)$ is the complex conjugate of $X_i(f_K)$ and $Y_i(f_K)$ represents a discrete approximation of the finite Fourier transform of the signal $y_i(t)$. The final estimate of the cross-spectral density function has been expressed as a statistical average over $q = 200$ samples, i.e.

$$\tilde{G}_{xy}(f_K) = \frac{1}{q} \sum_{i=1}^{q} \tilde{G}_{xy}(f_K). \qquad [A.10]$$

The coherence function, the system gain and phase factors, have been estimated as follows:

$$\hat{\gamma}_K^2 = \frac{|\tilde{G}_{xy}(f_K)|^2}{\tilde{G}_x(f_K) \cdot \tilde{G}_y(f_K)}, \qquad [A.11]$$

$$|\hat{H}(f_K)| = \frac{|\tilde{G}_{xy}(f_K)|}{\hat{G}_x(f_K)} \qquad [A.12]$$

and

$$\hat{\Phi}(f_K) = \tan^{-1}\left[\frac{\hat{Q}(f_K)}{\hat{C}(f_K)}\right], \qquad [A.13]$$

where $\hat{G}_y(f_K)$ represents the estimate of the power spectral density function of the signal $y(t)$. The quantities $\hat{Q}(f_K)$ and $\hat{C}(f_K)$ are defined by the following equation:

$$\hat{G}_{xy}(f_K) = \hat{C}(f_K) - j\hat{Q}(f_K). \qquad [A.14]$$

The coherence function defined by [A.11] is bounded to the range [0, 1], and is zero for completely uncorrelated signals and unity for completely correlated signals. The system gain factor [A.12] is < 1 if the coherent part of the signals is attenuated and is > 1 if the coherent part of the signals is amplified.